JOURNAL OF SPACECRAFT AND ROCKETS
Vol. 30, No. 2, March-April 1993

Particle Sightings by the Infrared Telescope on Spacelab 2

J. P. Simpson,* F. C. Witteborn,† and A. Graps‡
NASA Ames Research Center, Moffett Field, California 94035
G. G. Fazio§
Smithsonian Astrophysical Observatory, Cambridge, Massachusetts 02138
and
D. G. Koch¶
NASA Ames Research Center, Moffett Field, California 94035

Part of the objective of the cooled infrared telescope on Spacelab 2 was to determine the particle environment around the Space Shuttle. The telescope scanned the sky in six wavelength bands ranging from 2 to 100 μm with high time resolution. Dust particles could be identified from their particular signature in the data stream. Particle data from about 4 h early in the mission were analyzed in terms of size, color temperature, velocity, and time. The 1100 particles that were seen were slow moving and ranged in color temperature from 190 to 350 K with a few much hotter. The minimum detectable diameter is between 5 and 15 μm, depending on temperature. The size distribution resembles sample distributions collected at a Shuttle preparation facility. Although particle detection rates varied widely with time, no specific events were identified to be associated with particle production. It was not possible to determine the particle composition, although it was probably not ice.

Nomenclature

a	= particle radius
$B(T, \lambda)$	= blackbody function, $2hc^2\lambda^{-5}/(e^{hc/\lambda kT} - 1)$
D_A	= angular diameter of an out-of-focus image
D_T	= telescope diameter
d	= distance to particle
T	= particle temperature
$V1$	= average velocity
$V2$	= upper limit to particle velocity
$V3$	= lower limit to particle velocity
λ	= wavelength of light

Introduction

SPACE would seem to be the ideal astronomical observing site, especially at infrared wavelengths, since absorption and emission of photons by the terrestrial atmosphere is negligible. The spacecraft itself, however, produces sources of foreground radiation through the outgassing of molecules and the occasional release of particles. A discussion of the anticipated infrared foreground from Shuttle contaminant releases and their interaction with the Earth's low orbit environment is given by Simpson and Witteborn.[1] Particulates presented a major uncertainty because of lack of understanding of their sources. Clifton and Owens[2] showed from visible light camera observations that particles were indeed present in the near Shuttle environment. The infrared telescope (IRT) on Spacelab 2 provided the first test of the Shuttle as an infrared site. The papers on IRT by Koch et al.[3,4] provided information on foreground radiation in six IR bands (2.0-3.0, 4.5-9.5, 6.1-7.1, 8.5-14, 18-30, and 77-115 μm, S, A, B, C, D, and E, respectively) and estimated sizes and temperatures of nine particles observed during a short period of the flight. Here we present a more complete analysis of the 1100 particles observed by IRT and determine distributions in temperature, size, velocity, and distance of passage. Such distributions may be used to characterize the sources of particles and serve as a starting point for predicting particle production rates in future Shuttle missions.

First, we will estimate the angular velocities of the 280 particles for which we have good detections on more than one detector and their distances from the sizes of their out-of-focus images. Next, we will consider the 247 particles that were detected in both long (100 μm) and short (7 μm) bands. From the two fluxes, both the particle temperature and the diameter can be estimated. For a first approximation, we assume that the particles radiate as blackbodies and that all of the observed light is thermal emission with no scattering of radiation from the sun, Earth, or Shuttle. Next, we consider whether the particles would look different if they exhibited scattering properties of some real materials: water ice, Shuttle tile, graphite, magnetite, or aluminum oxide. Calculations of both the emitted and scattered light are described for spheres of these materials. None of the observed particles has a 100 μm/7 μm flux ratio as large as water ice particles would have, but some (5-10% of 247) have this 100 μm/7 μm ratio larger than predicted for the materials graphite, magnetite, or aluminum oxide, all of which are good scatterers at 7 μm. The last section compares the resulting size distribution with theoretical distributions and observed clean room distributions.

Instrument Description

The small helium-cooled infrared telescope flew on Spacelab 2 (Shuttle flight 51-F) in July-August 1985. Launch occurred at 21:00 GMT on day-of-year 210, and observing started at 19:40 of day 212. Koch et al.[3] have described the telescope operations and detector characteristics. The telescope was situated in the middle rear of the Shuttle bay (see Fig. 1 of Ref. 3). It scanned 45 deg to either side of the vertical toward the Shuttle wings at a rate of 6 deg/s, completing two

Received Jan. 21, 1992; revision received June 9, 1992; accepted for publication June 19, 1992.

*Research Astronomer, Astronomy Department, University of California, Berkeley, CA. Mailing address: NASA Ames Research Center, MS 245-6, Moffett Field, CA 94035-1000.

†Chief, Astrophysics Branch, Space Science Division, MS 245-6.

‡Software Specialist, Sterling Software, Palo Alto, CA. Mailing address: NASA Ames Research Center, MS 245-6, Moffett Field, CA 94035-1000.

§Senior Physicist, Optical and Infrared Astronomy, 60 Garden Street.

¶Research Scientist, Astrophysics Branch, Space Science Division, MS 245-6.

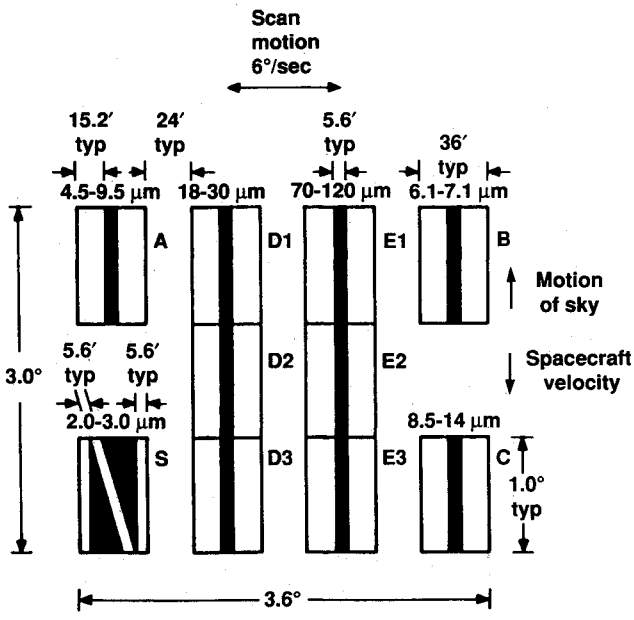

Fig. 1 Projection of the focal plane onto the sky.

full scans/min. The orbital motion of the Shuttle flying in airplane mode (nose in the direction of orbital motion and payload bay verticle pointed toward the zenith) produced an orthogonal angular motion of 4 deg/min. The combined motion enabled the telescope to cover 60% of the sky in each orbit. A sketch of the focal plane is shown in Fig. 1. The masks, bandwidths, angular sizes, and orientation of the 10 detectors are shown. Each detector viewed 0.6 deg in the direction of the scan, and 1.0 deg in cross scan. The sample rate was 1024 samples/s, later smoothed to 128 samples/s. There was a mask across each detector, with the result that when a point source was scanned, the resulting signal appeared double humped or "resolved." The signal from a dust particle so close that it was out of focus was not double humped and was therefore clearly distinguishable from point sources. For the IRT, a particle had an out-of-focus image size greater than the 0.6-deg detector size when it was closer than 14.3 m. Examples of data from a dust particle were shown in Ref. 3. The area in the vicinity of the galactic plane was not analyzed, as there are many extended sources that could be mistaken for dust particles.

In several instances, a resolved source appeared in one of the 100-μm detectors. Such a source is too cold to be a star unless the star has an extensive dust cloud. If it was not in the galactic plane (interstellar dust clouds are found in the galactic plane and are cold), the only other possible identifications are external galaxies (i.e., their dust clouds), planets and asteroids, and particles and space debris. For each such sighting, the Shuttle equation of motion was used to determine the coordinates on the sky for the source with an error of about 0.5 deg as determined from bright stars. The only galaxies securely identified were the bright far-IR galaxies M 82 and NGC 253. Jupiter was easily detected, but no bright asteroids. There were a few very small, faint asteroids within the error circles, but they were almost certainly too faint to be the observed source. A total of 26 resolved sources were detected that could not be identified as galaxies, planets, or galactic plane dust clouds; these sources were probably particles at distances larger than 14.3 m. Fourteen of these appeared as pairs; that is, they were probably only seven particles each appearing twice. Thus, the total is 19 resolved particles, a small fraction of the out-of-focus particles observed.

Data Analysis—Velocities

From the detector layout as shown in Fig. 1, it can be seen that as the telescope scanned, a stationary source on the celestial sphere would appear successively in each detector on a row. A short time later, on the next scan as the Orbiter pitched on the sky, the source would appear in the detectors in the next row, and so forth. Because of the constant scan rate, a fixed celestial source had a precise time difference between its appearances in two detectors in a given row (e.g., 0.50 s for detectors A and B). For a moving particle, angular velocity in the scan direction appeared as a difference between the measured and the normal (fixed celestial source) time between appearances in successive detectors in a row. Angular velocity in the cross-scan direction appeared as nonuniform coverage (i.e., substantially different fluxes) in the A and B detectors (which were in a row and had essentially the same effective wavelength) or as appearance in two detectors in different columns. Unfortunately, at no time were all detectors unsaturated.[3] We analyze here the data taken on day-of-year (DOY) 212, the only day when the A, B, and E1 detectors were working within their operating ranges. The single C and all three D detectors were saturated by the background (they had less dynamic range than the others), and thus the working detectors were S, A, B, E1, E2, and E3.

The distances to the particles can be estimated from the sizes of the out-of-focus images $D_A = D_T/d$, the diameter of the telescope D_T is 15 cm. The angular diameter was estimated from the length of time it took for the out-of-focus image to cross over a detector (as compared to a point source), or from the appearance of the image in several detectors simultaneously.

From the distance and the angular velocity, the linear velocity was readily found. Figure 2 displays the number of particles per linear velocity range. The velocity is the absolute

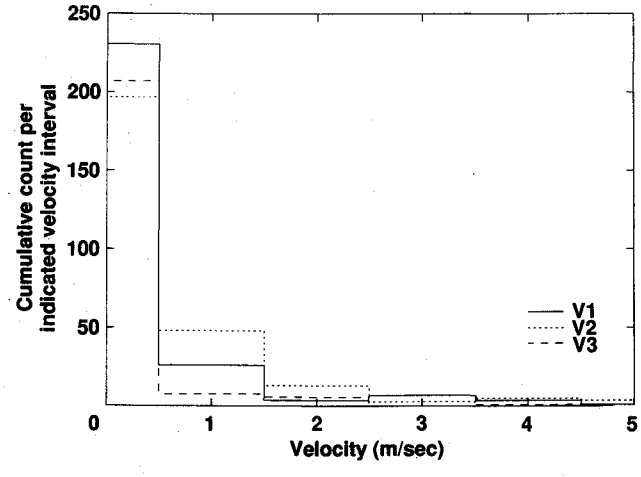

Fig. 2 Numbers of particles in various velocity intervals plotted vs velocity for the three measures of particle velocity described in the text.

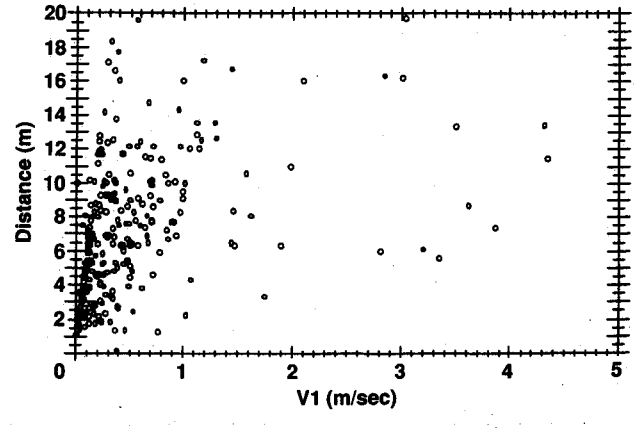

Fig. 3 Distance is plotted as a function of velocity for each particle.

magnitude of the sum of velocity components in the scan and cross-scan directions. Only upper and lower limits to cross-scan velocity could be determined. $V1$, $V2$, and $V3$ represent the velocity calculated using the average of upper and lower limits, the upper limit, and the lower limit, respectively, for cross-scan velocity added in quadrature to the scan velocity. It is clear that about two-thirds of the particles had velocities between 0 and 0.5 m/s. Of the 280 velocities measured, only one was as high as 38 m/s (upper limit). Between 20 and 70 of the 280 had velocities higher than 1.0 m/s. There was no obvious correlation between linear velocity and distance of particles (Fig. 3). About 72% of the particles with detectable cross-scan motion were moving toward the tail, the rest toward the nose. This could imply either that most of the particles were produced ahead (noseward) of the IRT, which was located near the tail end of the payload bay, or that air drag was affecting the trajectories of the particles observed. It was not possible to determine any radial motion toward or away from the telescope.

Data Analysis—Sizes and Temperatures

To determine the temperature and size of a particle, one needs to measure the emission at two widely different wavelengths. In this section, we assume that the particles radiate as blackbodies. In the next section, we will examine the error in temperature introduced by the blackbody assumption. We will see that for likely materials, this assumption introduces errors in temperature on the order of $\pm 20\%$ and in size on the order of less than $\pm 40\%$, and that the actual material cannot be determined.

From the ratio of the emission at the two wavelengths, one can calculate a "color" temperature; i.e., the blackbody temperature defined by the ratio of the fluxes at the two wavelengths. Then, under the assumption that the particle is a sphere emitting as a perfect blackbody, the equivalent diameter can be calculated from the observed flux at one of the two wavelengths, since the flux reaching a detector is independent of particle distance for out-of-focus particles.[1] The column of detectors closest to the tail of the shuttle contained detectors A (4.5–9.5 μm), E1 (77–115 μm), and B (6.1–7.1 μm). Detectors C (8.5–14 μm) and D (18–30 μm) were saturated on DOY 212. Detector S, at 2.0–3.0 μm, was at too short a wavelength to see blackbody emission from particles at the temperatures found in near Earth orbit, although it detected many particles in scattered sunlight. Although detector E1 had about half of the responsivity of detectors E2 and E3 and its responsivity was somewhat variable, because it was in line with A and B and had relatively little noise in its continuum level, it could be used for temperature determination. The minimum particle size in the figures, about 20 μm, corresponds to the minimum detectable flux in detector E1. There were many particles with easily detectable fluxes in detectors A and B that could not be detected in E1. The minimum detectable diameter for these particles is between 5 and 15 μm, depending on temperature. Lower limits to the particle temperatures were calculated for a few of the brightest (hottest) of these.

For each particle with both a short- (A or B) and a long- (E) wavelength detection, the fluxes were calibrated by comparing the detector signal to the signal measured from known astronomical sources: the stars α Her, G Her, and μ Cep for the short-wavelength bands[4] and the galaxies NGC 253 and M 82 for the long band. There were 247 particles with measurable temperatures; this represents 22% of the total number of particles detected.

The calculated color temperature of each particle is plotted as a function of time (in seconds of day 212) in Fig. 4, and the particle size as a function of color temperature is plotted in Fig. 5. The sizes are in some cases underestimated because it was assumed that the out-of-focus image of the particle completely covered the detector. (The sizes are certainly underestimated for the 11 resolved particles with both short- and long-wavelength data, and hence derived color temperatures. We

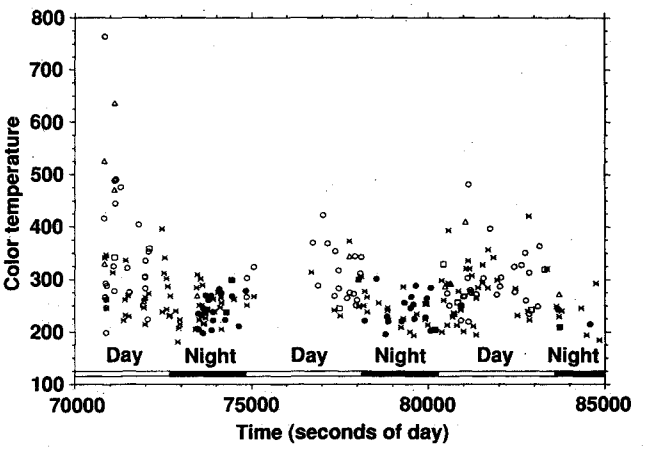

Fig. 4 Color temperature plotted as a function of elapsed time in day of year 212 for each particle.

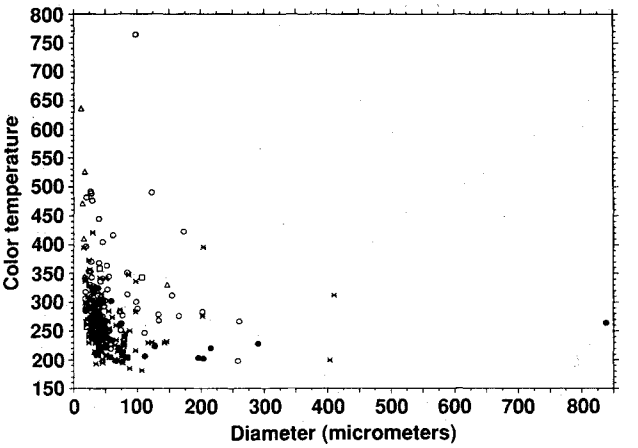

Fig. 5 Color temperature plotted vs diameter for each particle.

note that the temperature distribution for these resolved particles is the same as that of the unresolved out-of-focus particles, thus confirming their identification as particles, or at least objects in Earth orbit.) The squares represent the best data, that is, negligible cross-scan velocity which can be seen in that detectors A and B measured the same flux. The circles are for data with moderate cross-scan velocity (the fluxes for A and B were different, but a weighted average could be determined for comparison with detector E1). Triangles represent particles with good A and B fluxes but no E1 detection (since a change in the E1 response of one count could usually be detected, which typically was about 5×10^{-18} W cm^{-2} μm^{-1}). Thus, the plotted color temperatures are all lower limits for these hot particles. Sometimes the E2 or E3 flux was very much larger than the E1 flux. This might be caused by the center of the out-of-focus image of a very close particle passing over the E2 or E3 detectors and only the edge of the image passing over A, B, and E1; for these cases the largest E flux was used for determining the particle size, but not the temperature which was calculated from A, B, and E1. These particles are also represented by circles. Finally, the crosses are for particles where there was so much cross velocity that only A or B had good detections, but not both, or the crosses represent the particle detections on the one data tape containing no E1 data. The filled circles and squares are for times when the Shuttle was on the night side of the Earth, and the open circles are for times when the Shuttle was on the day side. Note that the hotter particles are all in sunlight.

Since all of the groups seem to have similar temperature distributions, we have combined them all together in Fig. 6, which is the number of particles in each 10 K temperature bin

as a function of temperature. (This is a selected sample of the higher quality color-temperature measurements. The full sample has the same shape and same trends, but slightly greater temperature scatter.) The high-temperature tails of both the day side and the night side distributions are real and not due to data with large error bars. They are the particles with good A and B fluxes but very low or no E1 detection. If these high color temperatures really indicate the true temperatures of the particles, these particles could not be in equilibrium, but must have been emitted from the Shuttle at some very high temperature and were cooling by radiation. For example, Barengoltz[6] showed that micrometeorites will spall off pieces of the surface layer of the Shuttle insulating tiles. These particles will initially be at high temperatures because of the high energy involved. Most of the particles produced by spallation are small and are moving too fast to be detected here. An interesting correlation is that the highest temperature particles were all detected at relatively small angles from the sun—from 49 to 70 deg. This would imply that forward scattering from the sun was significant. We will return to this point later in the next section.

Analysis—Possible Materials

It is clear that the particles on the night side of the Shuttle were colder than those on the day side, although there was a substantial overlap. The spreads of temperature are probably indicative of the particles being made of several different materials, which have substantially different equilibrium temperatures. It has been suggested that the particles seen around the Shuttle include ice from the flash evaporators and water dumps, particles of unburned fuel, tiny chips of tile spalled by micrometeorites, dirt blown out with gas from vents, and grit generated by moving parts. Here we compare the observed 7- and 100-μm fluxes with those predicted for spherical particles of various possible materials.

We have calculated the temperatures that small spherical particles would have in equilibrium in the environment of the Shuttle. The input energy includes thermal radiation from the sun (on the day side), the Earth, and the Shuttle, and sunlight scattered from the Earth and Shuttle. The absorptivity/emissivity as a function of wavelength was calculated with a Mie scattering program with the appropriate complex index of refraction. The input energy to the particle is equal to

$$\pi a^2 \int_0^\infty Q_{\text{abs}}(\Omega_\odot B_\odot + \Omega_\oplus B_\oplus + \Omega_{\text{Sh}} B_{\text{Sh}})\, d\lambda$$

and the energy emitted from the particle is given by

$$4\pi a^2 \int_0^\infty Q_{\text{abs}} \pi B_T\, d\lambda$$

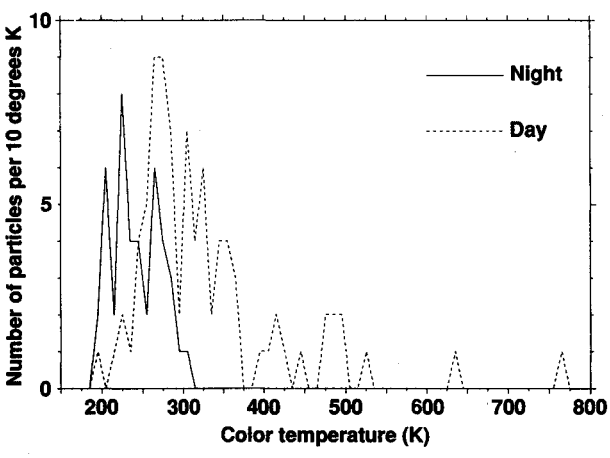

Fig. 6 Number of particles/10 K color-temperature interval plotted vs color temperature for night sightings and sightings in sunlight.

where Q_{abs} is the absorption efficiency as a function of wavelength λ and particle radius a from the Mie calculation; $\Omega_\odot$, $\Omega_\oplus$, and Ω_{Sh} are the solid angles of the sun, Earth (minus the amount obscured by the Shuttle), and Shuttle, and $B_\odot$, $B_\oplus$, B_{Sh}, and B_T are the blackbody functions at the temperatures of the sun, Earth (which is a function of wavelength because of the atmosphere), Shuttle (for which the hot radiators and bay must be distinguished from the cooler wings and fuselage), and particle at temperature T. By equating the input and output energies, the temperature T is determined. The results are that the equilibrium temperatures on the night side for all of the particles are cold, around 200 K. On the sunlight side, the material type is significant, because some materials are quite transparent to visible radiation (Q_{abs} small, $\lesssim 0.1$), while others are opaque ($Q_{\text{abs}} \sim 1.0$). For the dark (visible absorbing), nonvolatile materials, the daytime temperatures are in the range 300 to 340 K, with the larger (100 μm) particles hotter than the smaller ($a = 10$ μm). Materials transparent in the visible but not the infrared (like the glass that is used for the Shuttle insulating tiles, see Simpson and Witteborn[7]) have temperatures ranging from 240 to 280 K. Of course, ice particles are never in equilibrium because they are sublimating in the vacuum of space. Their predicted temperatures as a result are around 180 K in the Earth's shadow and a few degrees higher in sunlight. These estimates for ice are based on equating the energy absorbed from Earth, sun, and spacecraft to the energy of sublimation plus radiative emission.

With the exception of the high-temperature tails, the particles plotted in Fig. 4 fell in these ranges, although no particles were as cold as the 180 K predicted for ice. The reasons that one can compare color temperatures and physical temperatures are that the particles are large enough that the Q_{abs} or their ratios are not enormously different from unity and that the derived temperature is very insensitive to changes in the 7 μm/100 μm ratio because of the very large wavelength difference between the short- and long-wavelength bands. For example, the ratio of $B_{7\mu\text{m}}/B_{100\mu\text{m}}$ varies from 6.8 to 4600 as T varies from 180 to 600 K. Thus, changes in the 7 μm/100 μm ratio of a factor of two result in changes in the color temperature of only 9% at $T = 200$ K and 22% at $T = 400$ K. Likewise, the errors in the color temperature due to noise fluctuations are small, about 5 to 10 K for the larger 200 K particles and only 20 K for the smallest. Additional errors could arise in determining the baseline, or in assuming the particles were spherical when in fact many were obviously nonspherical (nonuniform emission) or were rotating.

One must also consider that color temperature does not mean equilibrium temperature. In addition to the flux radiated thermally by each particle, each particle also scatters radiation from the sun, Earth, and Shuttle into the telescope. The flux that would be radiated and scattered into the telescope was computed for different kinds of particles of different sizes and temperatures. Optical constants appropriate for ice,[8] Shuttle tile,[7] graphite,[9] magnetite,[10] and aluminum oxide[11] were used. Scattered light from the Earth, sun, and Shuttle was included, and all calculations were averaged over the wavelength response of the detectors and averaged over the appropriate scattering angle. Because the Shuttle was flying in airplane mode, the contributions from the Earth and Shuttle all come from the backscattering hemisphere. The scattering angle with respect to the sun ranged from 45 deg to about 110 deg. For ice and tile, the scattering efficiencies are much smaller than the absorption efficiencies. Thus, the scattered light contributions from the Earth, sun, and Shuttle were very small compared to the emitted contribution except at the coldest temperatures where they were of order 10–20%. For the graphite and magnetite particles, the scattering and thermal efficiencies are similar, so that the flux at 7 μm is dominated by scattered light for particle temperatures less than 230 K. The result is that no graphite and magnetite particles produce color temperatures lower than 196 K, and thus the very coldest appearing particles could not be graphite or magnetite.

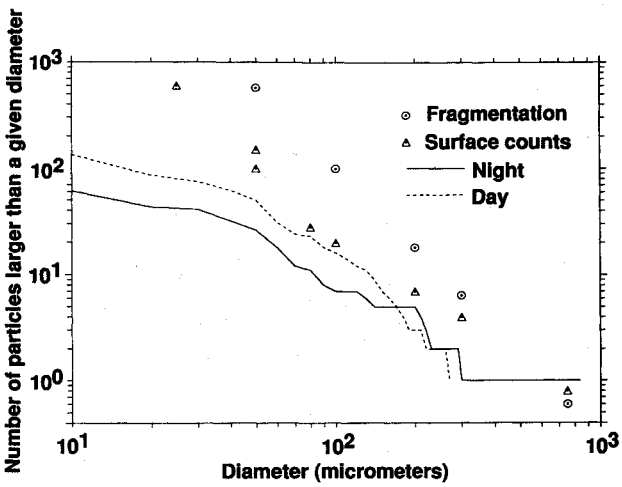

Fig. 7 Cumulative particle size distributions for day and night sightings compared with surface particle distribution observed during Spacelab 1 prelaunch checkout (triangles) and with a distribution associated with fragmenting solids (circles).

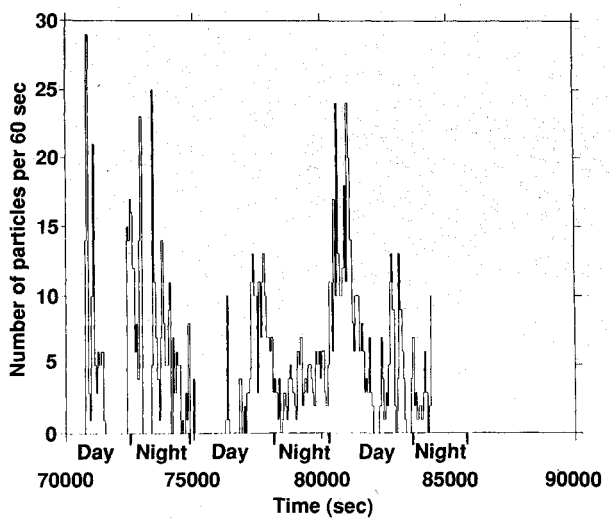

Fig. 8 Number of particle sightings vs elapsed mission time.

Aluminum oxide has the smallest imaginary part of the complex index of refraction at visible wavelengths and thus has the smallest absorption efficiency. Although aluminum oxide particles should be cold (~ 200 K) because they absorb so little at visible wavelengths, the observed cold particles could not be aluminum oxide because scattered light would dominate and give much higher color temperatures than true temperatures.

We return to the problem of the highest temperature particles. These were all detected at angles from the sun of 49–70 deg, perhaps indicating that forward scattering from the sun is significant. In the Mie scattering calculation from spheres just described, the forward scattering contribution from the sun at those angles is not large when compared to thermal emission for true particle temperatures above 350 K or for the materials considered here. On the other hand, specular reflection from flat surfaces ("glints") on a larger particle could produce the required excess 7 μm emission. The question, then, is what material can produce a specular reflection with scattering angle less than 70 deg but not greater? Another problem is that although some particles produce a signal on the detector that is very spikey with time (particularly at 2 μm) indicating reflection from a flat surface and rotation, such an appearance is not found in the particles with high color temperature.

We conclude that we cannot identify the material or materials which compose the observed particles. For this reason, all of the figures herein plot color temperature and diameter. We computed a matrix of flux at 7 and 100 μm as a function of particle size and temperature using the optical constants and scattering just described. Compared to the color temperatures and diameters, if the particles were magnetite or aluminum oxide, they would be smaller and hotter by up to 20%. Graphite particles would all be hotter, but the larger particles would be larger yet. The differences for Shuttle tile and ice would be similar: larger and cooler for the small particles, but smaller and hotter for the big particles. Since the coldest particles all get hotter for the ice optical constants, we still conclude that none of the particles are ice spheres.

Analysis—Particle-Size Distribution

Figure 7 shows the population of particle sizes. The population of small particle sizes is undoubtedly depleted by sensitivity selection effects although we did include those particles with 7 μm detections but no 100 μm detection. We may compare the measured distribution with measured particle fallout distributions on Spacelab 1 while in the Operations and Checkout Building at Kennedy Space Center[12] and with fragmentation distributions. We see that after allowance for undersampling for the smaller particles (since they are less likely to be detected by the IRT), the measured fallout distribution is a better match, but either one is acceptable.

Analysis—Time Dependence

Figure 8 shows the rate of particle sightings vs time. This period covers two sunrises and three sunsets. Sunlit (day) and Earth shadow (night) are denoted. The gaps are times when no data were taken. There appears to be no obvious correlation between orbital day/night and particle ejection rate. This tends to rule out thermal cycling as a particle ejection mechanism. Nearly 1100 particles were sighted during a total sampling time of 195 min. There was a detectable particle image somewhere on the focal plane about 3% of the time.

Conclusions

Sensitive infrared instruments using the Shuttle as an observing platform must be prepared for frequent particle sightings. (This situation may have been worse on Spacelab 2 which had nine separate experiments in the payload bay, some of which vented gas and some of which had exposed moving parts, than on a carefully controlled payload.) The particles sighted were slow moving with most velocities less than 0.5 m/s. The particles were too warm to be water ice. They were probably made of a variety of solids. They ranged in temperature from 190 to 300 K at night and from 200 to 350 K and higher in the day. The complete lack of hot particles at night plus the absence of any particles with velocities above 38 m/s rules out spallation by meteoroid impact as a contributor to the observed distribution of particles. Only 19 out of 1100 particles were more distant than 14 m from the telescope entrance; these particles are otherwise similar to the close particles and it is not determinable that any are "space debris," rather than particles produced immediately by Spacelab 2.

References

[1]Simpson, J. P., and Witteborn, F. C., "Effect of the Shuttle Contaminant Environment on a Sensitive Infrared Telescope," *Applied Optics,* Vol. 16, No. 8, 1977, pp. 2051–2073.

[2]Clifton, K. S., and Owens, J. K., "Optical Contamination Measurements on Early Shuttle Missions," *Applied Optics,* Vol. 27, No. 3, 1988, pp. 603–609.

[3]Koch, D. G., Fazio, G. G., Hoffmann, W., Melnick, G., Rieke, G., Simpson, J., Witteborn, F., and Young, E., "Infrared Observations of Contaminants from Shuttle Flight 51-F," *Advances in Space Research,* Vol. 7, No. 5, 1987, pp. 211–221.

[4]Koch, D. G., Melnick, G. J., Fazio, G. G., Rieke, G. H., Low, F. J., Hoffmann, W., Young, E. T., Urban, E. W., Simpson, J. P.,

Witteborn, F. C., Gautier, T. N. III, and Poteet, W., "Overview of Measurements from the Infrared Telescope on Spacelab 2," *Astrophysical Letters and Communications,* Vol. 27, No. 3, 1988, pp. 211–222.

[5] Fazio, G. G., "Small Helium-Cooled Infrared Telescope Experiment for Spacelab-2 (IRT), Final Report for Contract NAS8-32845," Smithsonian Astrophysical Observatory, Cambridge, MA, March 1990, p. 84.

[6]Barengoltz, J. B., "An Estimate of Particulates in the Vicinity of a Space Shuttle Orbiter due to Meteoroid Impacts," *Journal of Spacecraft and Rockets,* Vol. 17, No. 1, 1980, pp. 58–62.

[7] Simpson, J. P., and Witteborn, F. C., "Infrared Radiation from the Space Shuttle Contaminant Environment," *Proceedings of the USAF/NASA International Spacecraft Contamination Conference,* AFML-TR-78-190 or NASA-CP-2039, March 1978, pp. 176–207.

[8]Warren, S. G., "Optical Constants of Ice from the Ultraviolet to the Microwave," *Applied Optics,* Vol. 23, No. 8, 1984, pp. 1206–1225.

[9]Draine, B. T., "Tabulated Optical Properties of Graphite and Silicate Grains," *The Astrophysical Journal Supplement Series,* Vol. 57, March 1985, pp. 587–594.

[10]Lamy, P., Laboratoire d'Astronomie Spatiale, Marseille, France, private communication to O. B. Toon, NASA Ames Research Center, Moffett Field, CA, June 1979.

[11]Toon, O. B., Pollack, J. B., and Khare, B. N., "The Optical Constants of Several Atmospheric Aerosol Species: Ammonium Sulfate, Aluminum Oxide, and Sodium Chloride," *Journal of Geophysical Research,* Vol. 81, No. 33, 1976, pp. 5733–5748.

[12]Bareiss, L. E., Payton, R. M., and Papazian, H. A., "Shuttle/Spacelab Contamination Environment and Effects Handbook," NASA CR-4053, March 1987, pp. 2–19.

Alfred L. Vampola
Associate Editor